Implications of Low-Refractive Mode Index on Nonlinear Optical Interactions

Vertchenko, Larissa; Lavrinenko, Andrei

Published in:
Laser and Photonics Reviews

Link to article, DOI:
10.1002/lpor.202200741

Publication date:
2023

Document Version
Publisher's PDF, also known as Version of record

LASER & PHOTONICS REVIEWS
www.lpr-journal.org

Implications of Low-Refractive Mode Index on Nonlinear Optical Interactions

*Larissa Vertchenko and Andrei Lavrinenko**

Despite ample experimental evidence that the so-called epsilon-near-zero (ENZ) materials enable enhancement of nonlinear interactions in limited volumes of materials, there is still a lot of controversy about theoretical interpretation of results in search of optimal materials and structural configurations. The nonlinear performance of materials depending on their refractive index is compared and direct simulations prove with the indium-tin oxide material that the regime with low refractive index is superior to the ENZ regime in terms of the third harmonic generation (THG) efficiency. It is shown that as a rule for low-index materials the THG scales inversely proportional to the refractive index squared. Another advantage of low-index modes is that they satisfy phase-matching conditions by default. As exemplified by the direct numerical simulations, silicon-based photonic crystals can effectively produce third harmonic waves, which can be manipulated to propagate in any desired direction. Such an approach helps to avoid unnecessary complexity in on-chip linear and nonlinear circuitry and reduces potential sources of losses by unifying the whole production chain with implementation of the same material, e.g., silicon.

1. Introduction

Nonlinear optical processes are crucial for signal processing, storage, and optical communications being responsible for controlling light functions on chip.[1–4] Maximizing nonlinear interactions while decreasing the footprint of photonic devices is an ultimate goal of nonlinear photonics. For such applications, materials with pronounced change in the refractive index with a low intensity excitation are desired. However, nonlinear effects are linked to higher order electric susceptibilities $\chi^{(N)}$, which are very low for most of naturally available materials.[5] Consequently, bulky materials are employed aiming to increase the nonlinear interactions length. Changing the intrinsic susceptibility is extremely challenging, relying on complex fabrication techniques to conjugate multilayers of different composites. An alternative way to enhance nonlinear conversion efficiency is by nanoengineering materials promoting high concentration of electromagnetic fields in limited volumes.[6]

As shown in numerous studies, materials with vanishing relative permittivity ε referred to as epsilon-near-zero (ENZ) materials exhibit a set of remarkable properties, e.g., supercoupling through extremely distorted parts of waveguides,[7,8] quasistatic constant-phase propagation of fields,[9] absence of spontaneous emission, absence of a Doppler effect,[10] and extinction of any interference pattern.[11] Recently, there have appeared reports on facilitation of nonlinear interactions in the configurations, where ENZ materials are involved. [12–14] In particular, indium tin oxide (ITO) was reported to have a high induced change in refractive index about 0.7, evidencing improved strength of light–matter interactions both in the linear and nonlinear regimes on the wavelengths close to the ENZ point.[15–17]

In reality, the permittivity of materials with a Drude-like zero-crossing point is complex as a consequence of the Kramers–Kronig relations.[18] This fact influences propagation of light as it brings intrinsic losses through the imaginary part of the wave number k. Such losses persist to exist even when submitting devices to cryogenic temperatures, as it was exemplified on TiN films cooled down to 1.5 K.[19] More practical solutions can be found within an all-dielectric platform. Dielectric materials typically do not exhibit an ENZ permittivity in their dispersion spectra. Nevertheless, specific photonic crystal configurations can provide Dirac-cones with degenerated modes around the Γ point [20,21] of the dispersion diagram. Such modes propagate in a nearly constant phase regime, which can be attributed to an effective refractive index n being very small, e.g., $n \ll 1$. Few publications reported on experimental validation of existence of such regimes either in periodically corrugated ridge waveguides [11] or in 2D photonic crystals. [22]

Modes at the Γ point are not propagating in the plane of photonic crystals. This fact is exploited for efficient surface emitting

L. Vertchenko, A. Lavrinenko
Department of Electric and Photonics Engineering
Technical University of Denmark
Ørsteds Plads, Bld. 345A, Kongens Lyngby DK-2800, Denmark
E-mail: alav@fotonik.dtu.dk

L. Vertchenko
Sparrow Quantum Ltd.
Blegdamsvej 104A, Copenhagen DK-2100, Denmark

The ORCID identification number(s) for the author(s) of this article can be found under https://doi.org/10.1002/lpor.202200741

DOI: 10.1002/lpor.202200741

lasers,[23] but can be a drawback for on-chip devices. By a slight shift of frequency in the vicinity of the Dirac-point it is possible to obtain simultaneously a very low effective refractive index and a nonzero in-plane propagation constant.[24] Since Dirac-cones are located above the light-line, corresponding electromagnetic modes are radiative. Intensive leakage of energy out of the photonic crystal region can be avoided by, for example, using the phenomenon of bound states in the continuum.[24–27]

As a matter of fact, ENZ and near-zero index (NZI) are nonidentical conditions, i.e., the dispersion diagram of a material might have an ENZ crossing point at a specific frequency, but due to the imaginary part of the permittivity, such frequency does not necessarily corresponds to the lowest real part of the refractive index. The question under discussion is: which of these conditions provides stronger enhancement of optical nonlinear effects? From one side, the ENZ regime increases the normal component of the electric field through the boundary conditions. From another, the nonlinear refractive index n_2 is directly dependent on the real part of n, but not ε. Furthermore, the complex permittivity in ENZ materials imposes a challenge to phase-matching conditions, whereas low refractive index modes automatically obey the phase-matching regime irrespective to orientation of pump, signal, and idler waves.[28–30]

The rest of the article is as follows. We discuss the benefits of the NZI regime over the ENZ regime in Section 2 supporting our conclusions by numerical simulations. We compare the generation of the third harmonic by high and low index materials with close third-order susceptibilities, e.g., AlGaAs and ITO. In Section 3, we elaborate this point further using a photonic crystal patch made of silicon pillars designed to provide effective NZI modes. Through robust modeling, we demonstrate generation of the third harmonic with nonconventional phase matching resulting in full flexibility in designing the output directions. Section 4 concludes the paper.

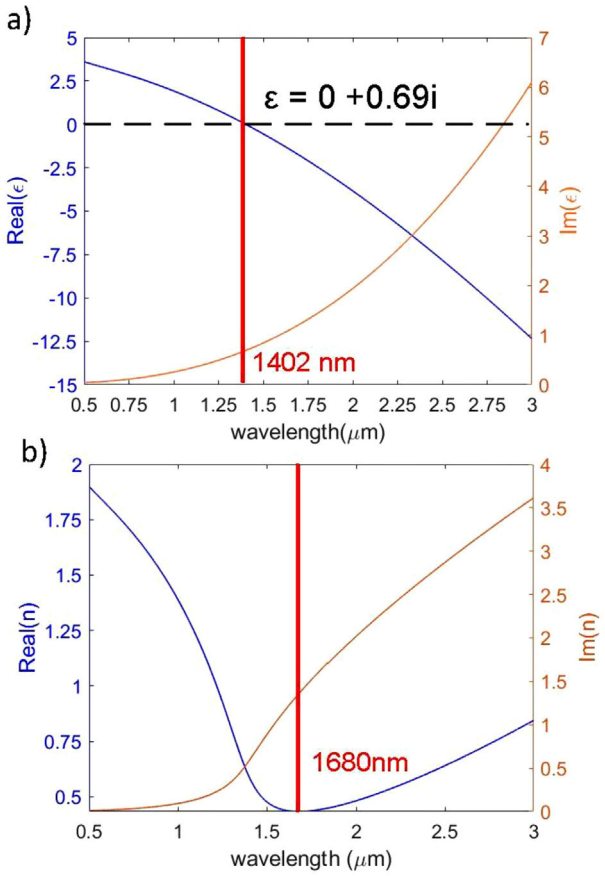

Figure 1. a) Complex permittivity and b) complex refractive index of an ITO film. The Drude–Lorentz parameters are acquired from.[34] The red solid vertical lines give the wavelengths of the ENZ and NZI regimes.

2. NZI Versus ENZ in Third-Order Nonlinearities

Kerr-like nonlinear optical processes related to the third order susceptibility $\chi^{(3)}$, such as third harmonic generation (THG) or four-wave mixing, can be quantified by the nonlinear refractive index n_2[13]

$$n_2 = \frac{3\chi^{(3)}(\omega)}{4n_0 Re\left(n_0\right)\varepsilon_0 c} \tag{1}$$

where n_0 is the linear refractive index on the fundamental frequency, c is the speed of light, and ε_0 is the vacuum permittivity. One obvious direction in improving of the THG is decreasing the effective refractive index. Knowing that the relative permittivity is connected to the linear refractive index by $n_0 = \sqrt{\varepsilon}$, we can speculate on n_2 enhancement by using ENZ materials. Of course, as this formula was derived through the perturbation theory, its direct application in the case of a very small refractive index is questionable. Nevertheless, it points out that low refractive indices (and not exactly ENZ, which with the use of realistic materials with complex permittivity can significantly deviate the refractive index from zero) are beneficial for more efficient THG and other nonlinear processes. Another positive factor for NZI materials can be low group velocities compressing E fields for high values.[31]

To elucidate which of the conditions, ENZ or NZI, enables higher THG we look on the material base. There are indisputable experimental observations showing that even a thin layer of an ENZ material around the fundamental harmonic wavelength ameliorates the third harmonic generation. [15,17,32,33] Typically, the material used in such experiments is ITO, but it optical properties depend on fabrication processes, for example, annealing temperature, and thickness of the deposited film. The maximum intensity of the THG was observed when the fundamental harmonic wavelengths coincided with the ENZ wavelengths.

Taking the parameters of the Drude–Lorentz model retrieved from ellipsometry data for an ITO film in reference,[34] we plotted the dispersion of the complex permittivity ε and complex refractive index n of the ITO film (**Figure 1**). As seen, the ENZ and NZI wavelengths ($\lambda_{ENZ} = 1402$ nm and $\lambda_{NZI} = 1680$ nm) are notably different. To conclude which of these regimes enables higher intensities of the third harmonic, we employed explicit time-domain nonlinear simulations with the finite-diffference time-domain (FDTD) Maxwell's solver (Lumerical) [35] following the method from Koos et al.[36] The simulated system consists of a 2 μm long patch of ITO with $\chi^{(3)} = 1.556 \times 10^{-18}$ m^2 V^{-2}. A pump excites the system in sequence on both wavelengths,

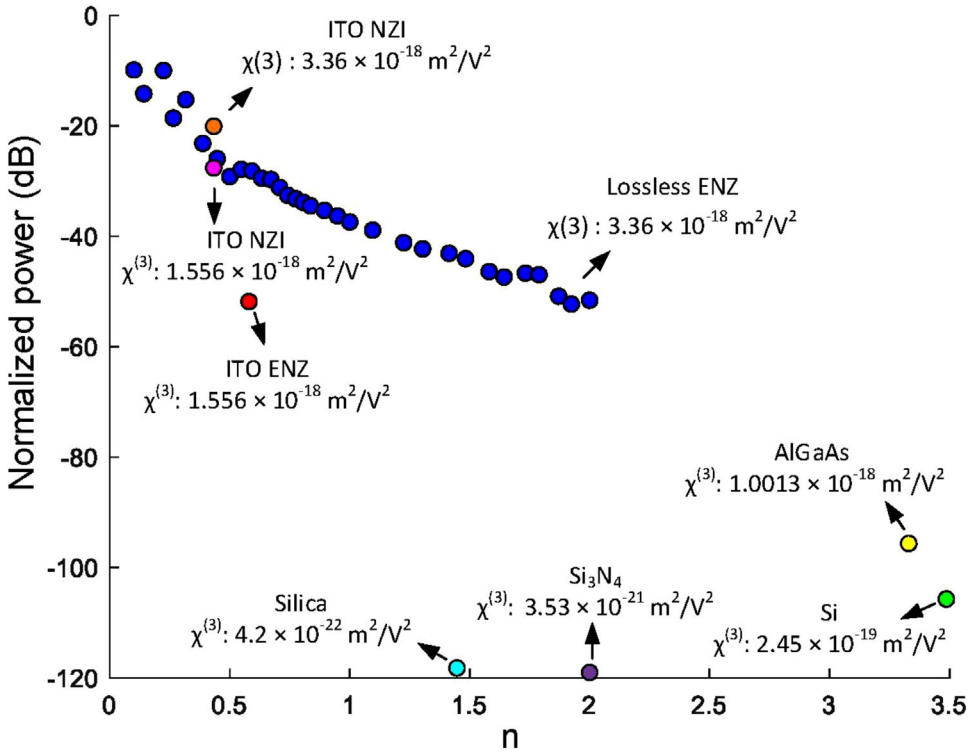

Figure 2. Normalized power of the third harmonic generated as a function of the linear refractive index at $\lambda = 1680$ nm for some materials (ITO, Silica, Si_3N_4, AlGaAs, and Si) with their respective values of susceptibility. As exception, the red point for ITO ENZ had the pump wavelength at $\lambda = 1402$ nm. Blue dots–normalized third harmonic power for a fictitious lossless ENZ material having the same third-order susceptibility ($\chi^{(3)} = 3.36 \times 10^{-18}$ m^2 V^{-2}) but decreasing linear refractive indices.

and a detection monitor is placed after the patch to quantify the converted signal. A more detailed explanation of the numerical methods can be found in the Supporting Information. The results are shown in **Figure 2**, where we plot the dependence of the normalized power of the THG signal versus the refractive index. It is clear that the conversion efficiency of n_{NZI} overwrites the n_{ENZ} case by more than 20 dB. The results are sufficiently interesting to stimulate a thorough experimental verification of this fact.

We continued our analysis by comparing the THG from conventional photonic materials (silica, silicon, AlGaAs, Si_3N_4) keeping the numerical domain layout with the same geometrical dimensions associated with the nonlinear materials and using the pump wavelength $\lambda_{NZI} = 1680$ nm. The THG intensities from ITO by far outperformed the other materials due to the interplay of higher $\chi^{(3)}$ value and lower refractive index. However, the direct comparison of nonlinear susceptibilities of ITO and AlGaAs shows only 50% exceeding in values of ITO, which cannot be responsible for such extended difference in the output THG (about 60 dB). One can see much less variation in Si and AlGaAs THG with the 4-times difference in $\chi^{(3)}$and very close refractive indices. This fact emphasizes the importance of a low refractive index regime.

To have further insight into the interplay between linear (refractive index n) and nonlinear $\chi^{(3)}$parameters we modeled the nonlinear response of another ITO film reported to have more than doubled $\chi^{(3)} = 3.36 \times 10^{-18}$ m^2 V^{-2}, [37] but keeping the same refractive index dispersion. As expected from the direct dependence between the susceptibility and n_2 the material with higher $\chi^{(3)}$ shows only 10-dB higher THG.

Finally, we extend our investigation by simulating fictitious materials having the same $\chi^{(3)} = 3.36 \times 10^{-18}$ m^2 V^{-2}, but different n without intrinsic losses under the identical pumping conditions. In such case, the ENZ and NZI regimes are indistinguishable. The tendency of increasing nonlinear response with lowering the refractive index is evident from the sequence of blue dots in Figure 2. As only the normal incidence is applied in numerical analysis, there are not any direct field enhancement effects due to the boundary conditions.

The behavior of THG with reduction of the lossless ENZ material linear refractive index (blue dots in Figure 2) points on some inverse power proportionality between the refractive index and intensity of the third harmonic. We show in **Figure 3** the result of the curve fitting for the normalized power P_{out}/P_{in} data using function $\gamma = a/n^2$, where a is the fitting coefficient with value 0.001. The fitting curve evidences the inversed quadratic dependence of the THG on the linear refractive index as shown by Equation (1).

So far, we have not investigated the phase matching conditions to the system in question. Nonlinear optical generation in conventional materials always occurs in the phase-matched geometry. Considering weak linear material dispersion, the third harmonic beam copropagates with the pump beam due to the momentum conservation. In the NZI structures, modes possess very small wavenumbers and accordingly a uniform phase distribution throughout the whole piece of material, automatically

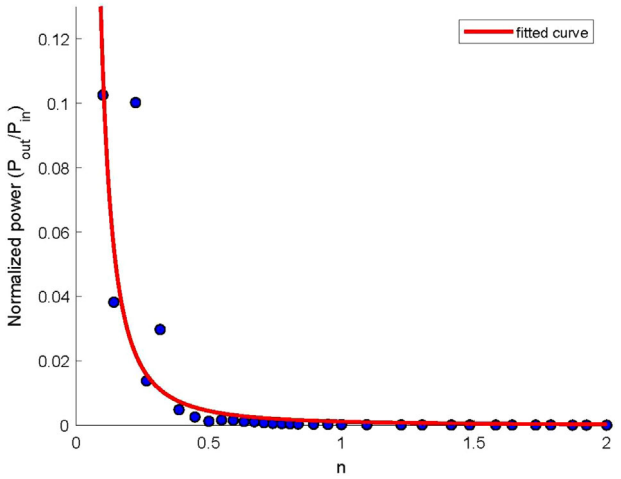

Figure 3. Normalized THG signal as a function of the linear refractive index. The red curve represents the fitting to function $y = a/n^2$, with a as a coefficient. The calculated root mean square error (RMSE) is 0.0149.

satisfying phase matching independently of the pump direction.[13,28] To prove the advantages of NZI materials with respect to generation of the third harmonic, we executed simulations with a uniform square patch with sizes ×5 μm^2. The detectors were arranged very close to each of the four boundaries. A monochromatic pump source operating at the NZI wavelength ($\lambda = 1680$ nm) is placed in free space at close proximity to the input (lower) boundary of the patch. The source excites the system by the linearly polarized pump beam propagating up in the vertical direction. We compared the nonlinear response resulted from the square patches made of Si ($\chi^{(3)} = 2.45 \times 10^{-19}$ m^2 V^{-2}), AlGaAs ($\chi^{(3)} = 1.00 \times 10^{-18}$ m^2 V^{-2}) and ITO ($\chi^{(3)} = 3.36 \times 10^{-18}$ m^2 V^{-2}). The indices of refraction of Si and AlGaAs were chosen accordingly to their tabulated dispersion properties on the fundamental wavelength. The simulations were performed in 2D configuration following numerical methods from Ref. [36]. We present our results in **Figure 4**. The first column shows broad spectral intensities caught by the upper detector placed in free space in front of the input one. Predictably, the third harmonic intensity is the highest for ITO, lower for AlGaAs, and almost negligible on the numerical noise level for Si. The second column exhibits results from the right output detector. As phase matching conditions are strictly violated for the case of high-index dielectrics, no distinct output is registered neither for the AlGaAs nor for the Si cases. However, a rather noticeable third harmonic propagates toward the right boundary of the low-index patch. The same effect was detected on the left side of the ITO patch. It is also noticeable that the intensity of the side-going third harmonic beams is somehow lower than that of the straight going one due to the shorter propagation path inside the nonlinear patch. Another interesting feature is the absence of Fabry-Perot fringes in the spectra of numerical noise for the low-index case as the fields in the whole patch bear the same phase, effectively extinguishing all interferometric effects.

To facilitate coupling out of the third harmonic we modernized the layout adding four identical slab silica waveguides to the 3 μm square patch. Pumping is done via the lower vertical waveguide; output intensity spectra are associated with the upper vertical and right horizontal waveguides. As expected, as shown in the Supporting Information, the third harmonic generated in the ITO patch has very similar intensities irrespectively of the waveguides position, while nothing special is seen for the silicon patch.

3. Third Harmonic Generation in a Photonic Crystal

The results shown in the previous sections emphasize the superior performance of low-index modes in nonlinear applications, in particular, the third harmonic generation in small footprint areas on-chip. However, these results were obtained with some numerical model approximations: uniform materials in simple shapes with prescribed dispersion properties. To show a practical way toward low-index nonlinearities having in mind fabrication specifications we exploited the concept of Dirac's triple point in a photonic crystal environment.[29] A triple-mode degeneration can lead to very low effective mode indices. There are few successful implementations of the Dirac (two linear and one flat dispersion) or semi-Dirac (at least one linear and one parabolic) modes exhibiting propagation within the NZI regime. [20,24] The latter case is preferential in terms of having a nonzero propagation constant for the in-plane modes in difference with the exact triple-degenerated Dirac Γ point.

Despite rather low nonlinear susceptibilities of pristine silicon, we decided to use it as a material platform to avoid challenges on fabrication routines and compatibility.[2] Also, its dispersion is robustly tabulated showing nice dielectric properties in the telecom ranges around 1300–1700 nm. We employed 2D simulations of silicon pillars surrounded by air. By optimizing the radius of the pillars ($r = 192$ nm) and pitch of the square lattice ($a = 921$ nm), we found an appropriate mode degeneration point at $\lambda = 1720$ nm, rather close to our previous pumping wavelength. For the sake of the CPU processing time, we took a 2D photonic crystal with sizes 17×17 lattice constants. To excite the system in a realistic way, we surrounded the system with another photonic crystal configuration with dimensions $r_m = 145$ and $a_m = 575$ nm. Such parameters were chosen aiming for a photonic bandgap around the pump and third harmonic wavelengths. The patch of the nonlinear-adjusted photonic crystal was embedded into the ambient photonic crystal bearing four line defects to be considered as input/output waveguides, see **Figure 5**. As before, monitors were placed in each waveguide near the NZI region, and a pump beam excites the THG from the bottom waveguide through its fundamental mode.

The electric field profiles are shown in the left column of Figure 5. Both fundamental and third-harmonic modes are effectively coupled out in all four waveguides. While coupling out of the fundamental harmonic is an ordinary fact, getting the third harmonic in all possible directions (even backward) is clear evidence of the quasi phase-matching enabled by the low-index propagating modes. The intensities of the third harmonic are almost the same in all four directions as illustrated by output spectra for the top and right waveguides (Figure 5b,d) and as can be viewed in the visualization color scheme in Figure 5a,c. The third harmonic outcoupling is far from being optimal as one can see intensive illumination outside the patch. Besides, the third-order

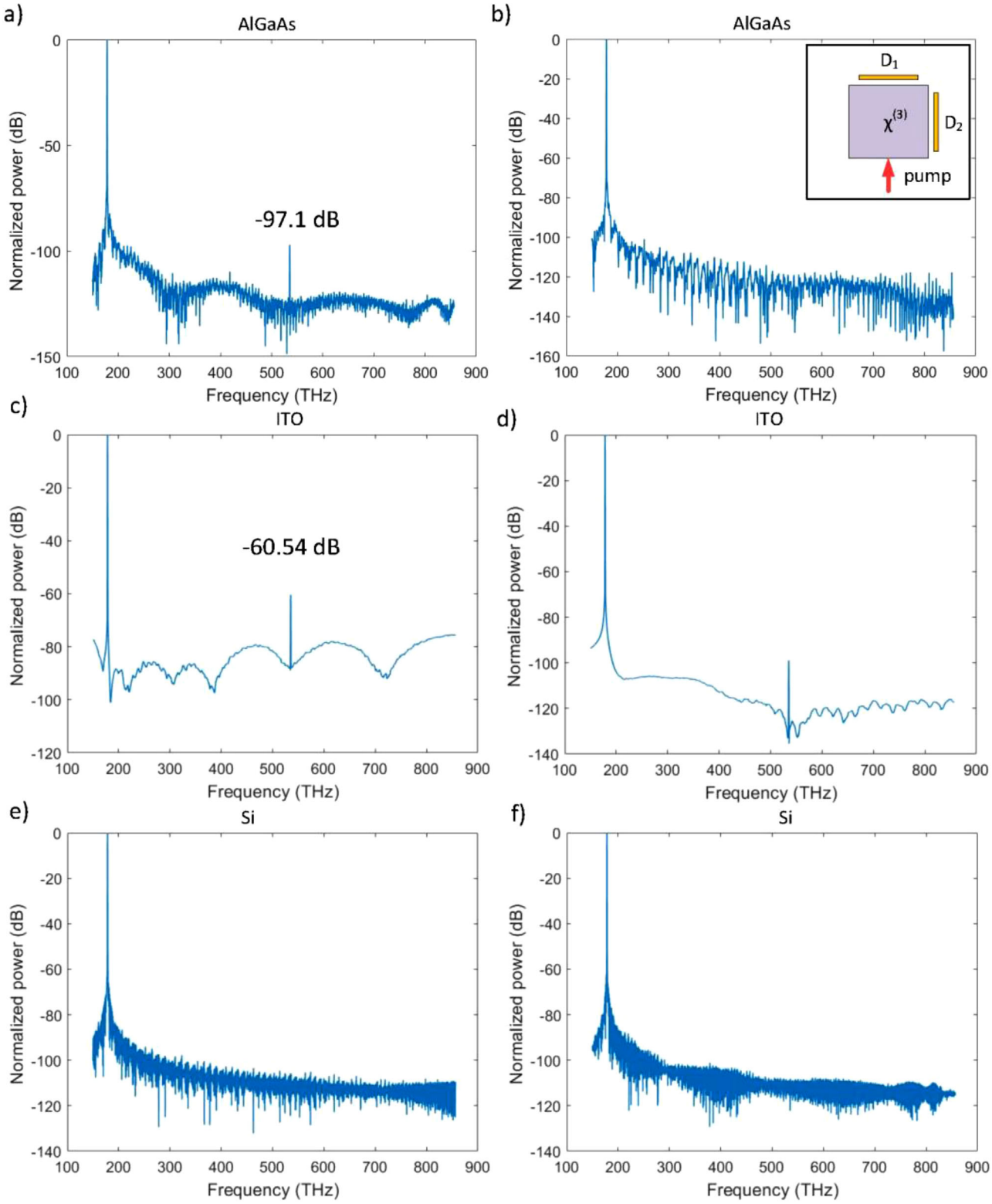

Figure 4. Spectra of output intensities from a 5×5 μm^2 patch made of a,b) AlGaAs ($\chi^{(3)} = 1.00 \times 10^{-18}$ m^2 V^{-2}), c,d) ITO ($\chi^{(3)} = 3.36 \times 10^{-18}$ m^2 V^{-2}), and e,f) Si ($\chi^{(3)} = 2.45 \times 10^{-19}$ m^2 V^{-2}). The first column (a,c,e) shows results from the upper detector (D_1), the second column (b,d,f) shows results from the right-hand detector (D_2). For an incident pump of frequency 178.448 THz (equivalent to wavelength 1680 nm), the third harmonic generation is predicted at the frequency 535.344 THz (equivalent to wavelength 560 nm). Inset: simulation layout. The pump beam with horizontal polarization comes from the bottom. The yellow lines designate position and sizes of detectors.

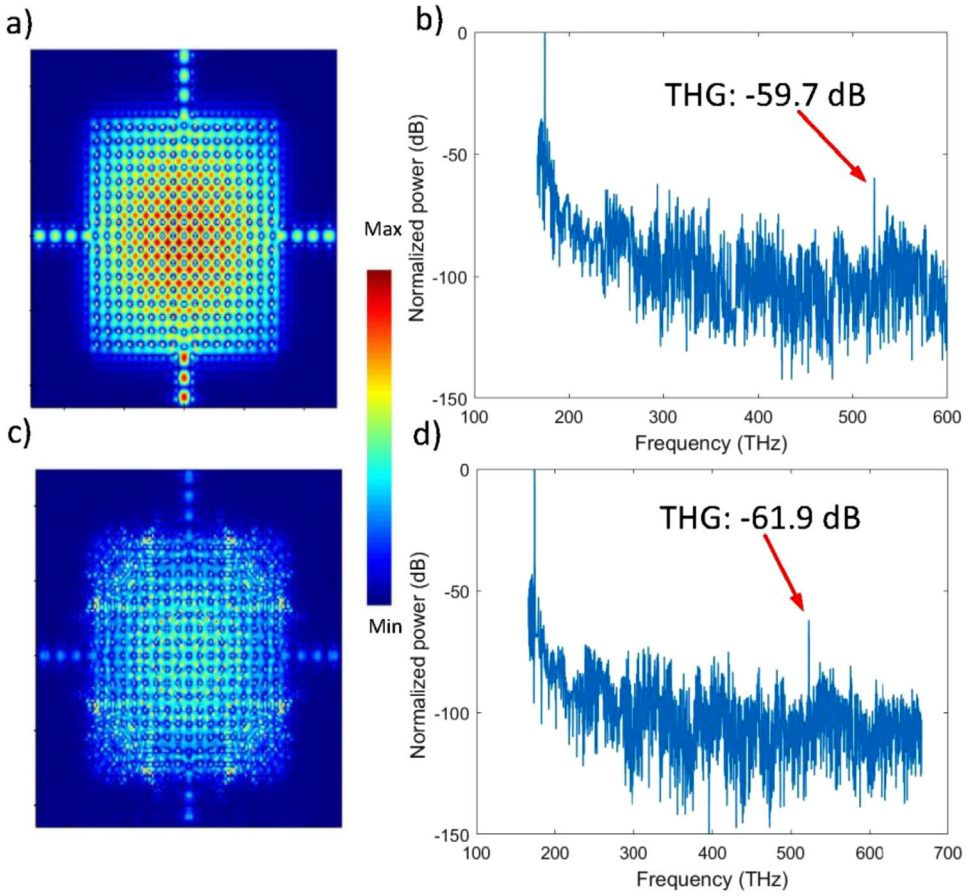

Figure 5. Electric field norm in the patch, waveguides, and ambient photonic crystal mirrors, a) at the fundamental harmonic wavelength $\lambda = 1720$ nm. b) Third harmonic intensities spectra in the top waveguide. c) Electric field norm in the patch at the third harmonic wavelength $\lambda = 573$ nm and d) intensities spectra in the right waveguide.

susceptibility in Si is notoriously quite moderate. Both factors together with a very small extension of the available nonlinear space significantly reduce the THG intensity. Nevertheless, the presence of the third harmonic generation and its tolerance toward the phase-matching conditions is proven and gives a place for further development of NZI dielectric platforms for nonlinear applications.

4. Conclusion

Despite the obvious experimental observations that both ENZ and NZI materials enhanced optical nonlinear effects, there is still some controversy surrounding the interpretation of the origin of such enhancements. Here we contributed to this discussion by brute force modeling of nonlinear effects, in particular the third harmonic generation, without making any assumption on the field strength, exploiting approximate formulas and any other analytical and numerical tricks conventionally used in such kind of nonlinear modeling.

Our findings first point out to the superior importance of the NZI regime over the ENZ one if there is a possible option to differentiate them, for example, by a wavelength range. Even with the same nonlinear susceptibility, the low-index materials more efficiently convert the fundamental harmonic in the third one. Therefore, the quasiphase-matching effect granted by default for a low-index mode is a powerful tool to facilitate nonlinear interactions especially in devices with a very limited on-chip footprint. Our following observation led to the conclusion that a conventional Si platform can be an appropriate choice for bringing nonlinear functions connected with control of light waves propagation on chip in the frames of silicon photonics. This is a point, where the matured cleanroom technologies can be directly applied to minimize unnecessary losses connected with fabrication imperfections. Finally, in unison with the four-waves mixing observations reported,[30] there is a freedom in arranging three- and four-waves interactions regarding propagation directions of signal and idler beams relative to the pumping beam orientation. This can be an extremely useful function for dense on-chip photonic contours lifting out requirements for rather long components under special arrangements and additional coupling and splitting elements.

5. Experimental Section

Numerical modeling: Simulations are performed using the commercial software Lumerical. Details of simulations are given in the Supporting Information.

Supporting Information

Supporting Information is available from the Wiley Online Library or from the author.

Acknowledgements

This work was supported by the Danish National Research Foundation through NanoPhoton – Center for Nanophotonics, Grant No. DNRF147. A.L. acknowledged the support from the Independent Research Fund Denmark, DFF Research Project 2 "PhotoHub" (No. 8022-00387B).

Conflict of Interest

The authors declare no conflict of interest.

Author Contributions

L.V. carried out the simulations and designed the samples. A.L. supervised the research. Both authors discussed the results and wrote the manuscript.

Data Availability Statement

The data that support the findings of this study are available from the corresponding author upon reasonable request.

Keywords

epsilon-near-zero, near-zero index, photonic crystal, third harmonic generation

Received: September 30, 2022
Revised: May 8, 2023
Published online: August 4, 2023

[1] D. Cotter, R. J. Manning, K. J. Blow, A. D. Ellis, A. E. Kelly, D. I. Nesset, D. Phillips, A. J. Poustie, D. C. Rogers, *Science* **1999**, *286*, 1523.
[2] J. Leuthold, C. Koos, W. Freude, *Nat. Photonics* **2010**, *4*, 535.
[3] Y. Zhao, X. Ji, B. Y. Kim, P. S. Donvalkar, J. K. Jang, C. Joshi, M. Yu, C. Joshi, R. R. Domeneguetti, F. A. S. Barbosa, P. Nussenzveig, Y. Okawachi, M. Lipson, A. L. Gaeta, *Optica* **2020**, *7*, 135.
[4] M. Pu, H. Hu, L. Ottaviano, E. Semenova, D. Vukovic, L. K. Oxenløwe, K. Yvind, *Laser Photonics Rev.* **2018**, *12*, 1800111248.
[5] A. Krasnok, M. Tymchenko, A. Alù, *Mater. Today* **2018**, *21*, 8.
[6] G. Li, S. Zhang, T. Zentgraf, *Nat. Rev. Mater.* **2017**, *2*, 1.
[7] M. G. Silveirinha, N. Engheta, *Phys. Rev. B* **2007**, *76*, 245109.
[8] N. Engheta, *Science* **2013**, *340*, 286.
[9] L. Vertchenko, N. Akopian, A. V. Lavrinenko, *Sci. Reports* **2019**, *9*, 6053.
[10] M. Lobet, I. Liberal, L. Vertchenko, A. V. Lavrinenko, N. Engheta, E. Mazur, *Light: Sci. Appl.* **2022**, *11*, 110.
[11] O. Reshef, P. Camayd-Muñoz, D. I. Vulis, Y. Li, M. Loncar, E. Mazur, *ACS Photonics* **2017**, *4*, 2385.
[12] L. Caspani, R. P. M. Kaipurath, M. Clerici, M. Ferrera, T. Roger, J. Kim, N. Kinsey, M. Pietrzyk, A. Di Falco, V. M. Shalaev, A. Boltasseva, D. Faccio, *Phys. Rev. Lett.* **2016**, *116*, 233901.
[13] O. Reshef, I. De Leon, M. Z. Alam, R. W. Boyd, *Nat. Rev. Mater.* **2019**, *4*, 535.
[14] M. Vincenti, D. de Ceglia, M. Scalora, *Opt. Express* **2020**, *28*, 31180.
[15] M. Z. Alam, I. De Leon, R. W. Boyd, *Science* **2016**, *352*, 795.
[16] N. Kinsey, C. DeVault, A. Boltasseva, V. M. Shalaev, *Nature Rev. Mat.* **2019**, *4*, 742.
[17] W. Jaffray, S. Saha, V. M. Shalaev, A. Boltasseva, M. Ferrera, *Adv. Opt. Photonics* **2022**, *14*, 148.
[18] M. H. Javani, M. I. Stockman, *Phys. Rev. Lett.* **2016**, *117*, 107404.
[19] L. Vertchenko, L. Leandro, E. Shkondin, O. Takayama, I. V. Bondarev, N. Akopian, A. V. Lavrinenko, *Opt. Mater. Express* **2019**, *9*, 2117.
[20] D. I. Vulis, O. Reshef, P. Camayd-Muñoz, E. Mazur, *Rep. Prog. Phys.* **2018**, *82*, 012001.
[21] X. Huang, Y. Lai, Z. H. Hang, H. Zheng, C. T. Chan, *Nat. Mater.* **2011**, *10*, 582.
[22] Y. Li, S. Kita, P. Muñoz, O. Reshef, D. I. Vulis, M. Yin, M. Lončar, E. Mazur, *Nat. Photonics* **2015**, *9*, 738.
[23] R. Contractor, W. Noh, W. Redjem, W. Qarony, E. Martin, S. Dhuey, A. Schwartzberg, B. Kanté, *Nature* **2022**, *608*, 692.
[24] L. Vertchenko, C. DeVault, R. Malureanu, E. Mazur, A. Lavrinenko, *Laser Photonics Rev.* **2021**, *15*, 2000559.
[25] C. W. Hsu, B. Zhen, A. D. Stone, J. D. Joannopoulos, M. Soljačić, *Nat. Rev. Mater.* **2016**, *1*, 1.
[26] M. Minkov, I. A. Williamson, M. Xiao, S. Fan, *Phys. Rev. Lett.* **2018**, *121*, 263901.
[27] T. Dong, J. Liang, S. Camayd-Muñoz, Y. Liu, H. Tang, S. Kita, P. Chen, X. Wu, W. Chu, E. Mazur, L. Yang, *Light: Sci. Appl.* **2021**, *10*, 10.
[28] H. Suchowski, K. O'Brien, Z. J. Wong, A. Salandrino, X. Yin, X. Zhang, *Science* **2013**, *342*, 1223.
[29] Y. Li, C. T. Chan, E. Mazur, *Light: Sci. Appl.* **2021**, *10*, 203.
[30] J. R. Gagnon, O. Reshef, D. H. Espinosa, M. Z. Alam, D. I. Vulis, E. N. Knall, J. Upham, Y. Li, K. Dolgaleva, E. Mazur, R. W. Boyd, *Phys. Rev. Lett.* **2022**, *128*, 203902.
[31] J. B. Khurgin, M. Clerici, V. Bruno, L. Caspani, C. DeVault, J. Kim, A. Shaltout, A. Boltasseva, V. M. Shalaev, M. Ferrera, D. Faccio, N. Kinsey, *Optica* **2020**, *7*, 226.
[32] A. Capretti, Y. Wang, N. Engheta, L. Dal Negro, *Opt. Lett.* **2015**, *40*, 1500.
[33] C. Liu, M. Z. Alam, K. Manukyan, K. Pang, Y. Zhou, H. Song, X. Su, J. R. Hendrickson, E. M. Smith, M. Tur, R. W. Boyd, A. E. Willner, *IEEE Photonics Conference* (IPC), Vancouver, BC, Canada, **2020**, pp. 1–2.
[34] G. V. Naik, V. M. Shalaev, A. Boltasseva, *Adv. Mater.* **2013**, *25*, 3264.
[35] "Lumerical Inc." https://www.lumerical.com/. (accessed: 6 July **2022**).
[36] C. Koos, M. Fujii, C. G. Poulton, R. Steingrueber, J. Leuthold, W. Freude, *IEEE J. Quantum Electron.* **2006**, *42*, 1215.
[37] J. L. Humphrey, D. Kuciauskas, *J. Appl. Phys.* **2006**, *100*, 113123.